Ab initio calculations of electron inelastic mean free paths and stopping powers

A. P. Sorini,[1] J. J. Kas,[1] J. J. Rehr,[1] M. P. Prange,[1] and Z. H. Levine[2]
[1]*Department of Physics, University of Washington, Seattle, Washington 98195, USA*
[2]*National Institute of Standards and Technology, Gaithersburg, Maryland 20899, USA*
(Received 5 May 2006; revised manuscript received 24 July 2006; published 20 October 2006)

A method is presented for first-principles calculations of electron inelastic mean free paths and stopping powers in condensed matter over a broad energy range. The method is based on *ab initio* calculations of the dielectric function in the long wavelength limit using a real-space Green's function formalism, together with extensions to finite momentum transfer. From these results we obtain the energy-loss function and related quantities such as optical-oscillator strengths and mean excitation energies. From a many-pole representation of the dielectric function we then obtain the electron self-energy and inelastic mean free paths. Finally, using our calculated dielectric function and the optical-data model of Fernández-Varea *et al.* [Nucl. Instr. and Meth. B **229**, 187 (2005)], we obtain collision stopping powers and penetration ranges. The results are consistent with semiempirical approaches and with experiment.

DOI: 10.1103/PhysRevB.74.165111 PACS number(s): 77.22.Ch, 34.80.−i, 34.50.Bw

I. INTRODUCTION

The effect of inelastic losses on fast electrons has long been of theoretical and experimental interest,[1–3] and continues to be an area of active development.[4–6] Theoretical calculations of such losses depend on the dielectric response of a material over a broad spectrum. Moreover, calculations of these losses are particularly sensitive to the excitation spectrum of a material. While first-principles approaches have been developed for calculations of losses at low energies, i.e., up to a few tens of eV,[7,8] these methods are computationally intensive and may be difficult to implement. Thus detailed calculations of inelastic losses have generally been limited to semiempirical approaches,[4,9–14] based on experimental optical data. On the other hand, experimental data over a sufficiently broad spectrum are not readily available for many materials of interest.

In an effort to overcome these difficulties, we present here a first-principles, real-space approach for general calculations of inelastic losses. The approach is applicable to both periodic and aperiodic condensed matter systems throughout the periodic table. Our calculations are based on *ab initio* calculations of the complex dielectric function $\epsilon(\omega)=\epsilon_1(\omega)+i\epsilon_2(\omega)$ as a function of the frequency ω, in the long wavelength limit, together with extensions to finite momentum transfer.[16] The calculations of $\epsilon(\omega)$ are carried out using an all-electron, real-space Green's function (RSGF) formalism as implemented in a generalization of the FEFF8 code[17,18] for full-spectrum calculations of optical constants. This generalization of the FEFF8 code is referred to as FEFF8OP below.

We focus in this paper on several physical quantities which characterize the inelastic interactions of a fast probe electron, a photo electron, or other charged particle in condensed matter. These include the inelastic mean-free-path (IMFP) and the collision stopping-power (CSP). Each of these quantities depends on the complex dielectric function $\epsilon(\omega)$ through the energy-loss function (ELF) for a given material $-[\mathrm{Im}\,\epsilon^{-1}(\omega)]=\epsilon_2(\omega)/[\epsilon_1(\omega)^2+\epsilon_2(\omega)^2]$, which is calculated here up to x-ray energies. The ELF is directly related to the optical oscillator strength (OOS). From the OOS, which characterizes the distribution of excitations (e.g., plasmons, particle-hole excitations, etc.), we obtain values of the mean excitation energy I. Recently a comprehensive relativistic treatment of inelastic losses and scattering within the first Born approximation has been developed by Fernández-Varea *et al.*[4] Their semiempirical approach requires experimental optical data as input, and is referred to here as the optical data model (ODM). This approach has the advantage that calculations of quantities such as the CSP are reduced to a single quadrature. To facilitate precise comparisons, we have used their formulation for our CSP calculations, except for the substitution of our *ab initio* dielectric function. Our approach is therefore referred to as the "*ab initio* data model" (ADM). We have also compared IMFPs calculated using both the ADM and a one-particle self-energy approach.

Formally the IMFP and the CSP are related to energy moments of the differential cross-section (DCS) for inelastic collisions $d\sigma/d\omega$ of a fast probe electron (or other charged particle) of initial kinetic energy E with energy loss ω. The inverse IMFP is proportional to the zeroth moment of the DCS

$$\frac{1}{\lambda(E)}=n_a\int d\omega\frac{d\sigma(\omega;E)}{d\omega}=n_a\sigma^{(0)}(E), \tag{1}$$

where n_a is the atomic number density. Here and elsewhere in this paper we use Hartree atomic units ($m=\hbar=e=1$). Thus distances are in Bohr ($a_0\approx 0.529$ Å) and energies in Hartree (H≈27.2 eV), unless otherwise specified. The CSP, here denoted by $S(E)$, is proportional to the first moment of the DCS

$$S(E)=n_a\int \omega d\omega\frac{d\sigma(\omega;E)}{d\omega}=n_a\sigma^{(1)}(E). \tag{2}$$

Since $S(E)=-dE/dx$, this quantity has units of force. From an integral of $1/S(E)$ over energy we can then obtain the so-called "continuous slowing-down approximation" (CSDA) penetration range $R(E)$ as

$$R(E) = \int_0^E \frac{dE}{S(E)}. \tag{3}$$

Implicit in Eqs. (1) and (2) are the kinematics of the colliding particles. In this paper we choose kinematics relevant for probe electrons. Regardless of the probe, the sample is characterized by the dielectric function $\epsilon(\mathbf{q},\omega)$. In this paper we consider cubic materials which we approximate as isotropic, i.e., in which the dielectric function depends only on the magnitude of the momentum transfer $q=|\mathbf{q}|$.

The DCS may be considered as the sum of longitudinal (instantaneous Coulomb) and transverse (virtual photon) contributions, denoted below with subscripts L and T, respectively. The detailed relativistic form of the relationship between each contribution to the DCS and the ELF is obtained by integrating the double differential cross-section (DDCS) over the kinematically allowed values of momentum-transfer,[4]

$$\frac{d\sigma(\omega;E)}{d\omega} = \int dq \frac{d\sigma(q,\omega;E)}{dqd\omega}, \tag{4}$$

where

$$\frac{d\sigma(q,\omega)}{dqd\omega} = \frac{d\sigma_L(q,\omega)}{dqd\omega} + \frac{d\sigma_T(q,\omega)}{dqd\omega}. \tag{5}$$

As an example of how the dielectric function determines the DDCS, we recall the familiar nonrelativistic result

$$\frac{d\sigma(q,\omega)}{dqd\omega} = \frac{d\sigma_L(q,\omega)}{dqd\omega} = -\frac{1}{2\pi n_a q v^2} \mathrm{Im}\ \epsilon^{-1}(q,\omega), \tag{6}$$

where v is the velocity of the probe electron. The relativistic analog of Eq. (6) is similar and is given explicitly in Eqs. (8) and (9) of Ref. 4.

One of the main goals of this work is to calculate mean excitation energies I and IMFPs for general condensed matter systems over an energy range up to about 100 keV. Another goal is to calculate CSPs and penetration ranges over a range of order 10 MeV. We compare our results both with semiempirical approaches and with experimental data and tabulations.

II. MODEL DIELECTRIC FUNCTION

Both the IMFP and the CSP can be computed as convolutions of the momentum-transfer and energy-loss dependent inverse dielectric function $\epsilon^{-1}(q,\omega)$, with relativistic weighting functions. The precise details of the weighting functions are discussed further below. In this section we discuss the extension of our *ab initio* calculation of $\epsilon(q,\omega)$ in the long wavelength $(q\to 0)$ limit to finite q.[4,9,19–21] In this work $\epsilon(\omega)\equiv\epsilon(0,\omega)$ is calculated from the UV to x-ray energies using the *ab initio* real-space Green's function code FEFF8OP,[18,22] which sums the contributions to the spectra over all occupied core and semicore initial states. As an example, the calculated ELF for Ag is shown in Fig. 1.

We have chosen to discuss the extension to finite q in terms of the ELF, but we could just as well have used the

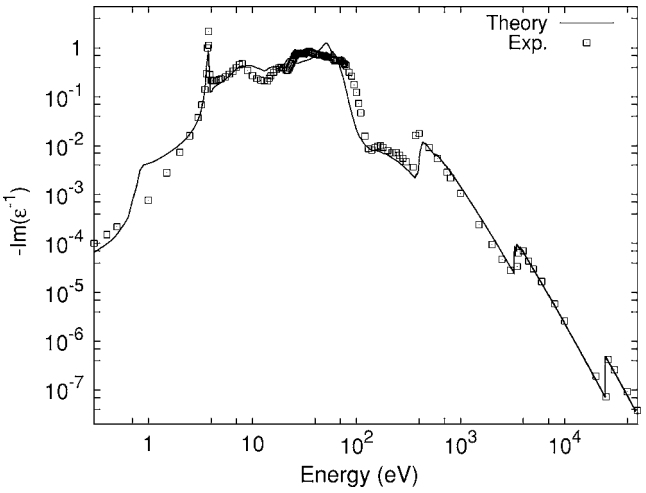

FIG. 1. The energy-loss function $-[\mathrm{Im}\ \epsilon^{-1}(\omega)]$ of fcc silver as calculated in this work (solid line) and from experiment (Refs. 23 and 24) (dots).

OOS $g(\omega)$, which differs by a factor proportional to ω, i.e.,

$$g(\omega) = -\frac{2}{\pi}\frac{Z}{\Omega_p^2}\omega\ \mathrm{Im}[\epsilon^{-1}(\omega)], \tag{7}$$

where $\Omega_p^2=4\pi n_a Z$ is the all-electron plasma frequency and Z is the atomic number. As an illustration of the quantitative agreement of our approach, three *ab initio* OOS calculations, spanning a range of atomic numbers, are compared to experiment in Fig. 2. Clearly the approximations in FEFF8, such as the use of atomic core initial states in the OOS calculation and muffin-tin scattering potentials, are adequate to yield good agreement with experiment for UV energies and above. Additional examples are tabulated on the WWW.[25] For optical frequencies and below, however, the agreement is only semiquantitative, but the errors tend to be suppressed in the OOS due to the overall factor of ω in Eq. (7). Further discussion of properties of our calculated OOS, including the f-sum rule, can be found elsewhere.[18,22]

A global measure of the excitation spectra is given by the "mean excitation energy" $\ln I=\langle \ln \omega\rangle$, where the "mean" $\langle\cdots\rangle$ refers to an average with respect to the OOS weighting function, i.e.,

$$\ln I = \frac{\int d\omega g(\omega)\ln\omega}{\int d\omega g(\omega)}. \tag{8}$$

The quantity I appears in expressions for the collision stopping power, as shown in Sec. V. below. In Table I theoretical values of I, as calculated from our OOS spectra, are compared with those calculated from experimental optical constants,[24] and also with internationally recommended (ICRU) values for several elements. For low Z elements, the theoretical values of I are clearly in good agreement with measured values. For high Z elements, I is predicted by the Thomas-Fermi models to be proportional to Z. The propor-

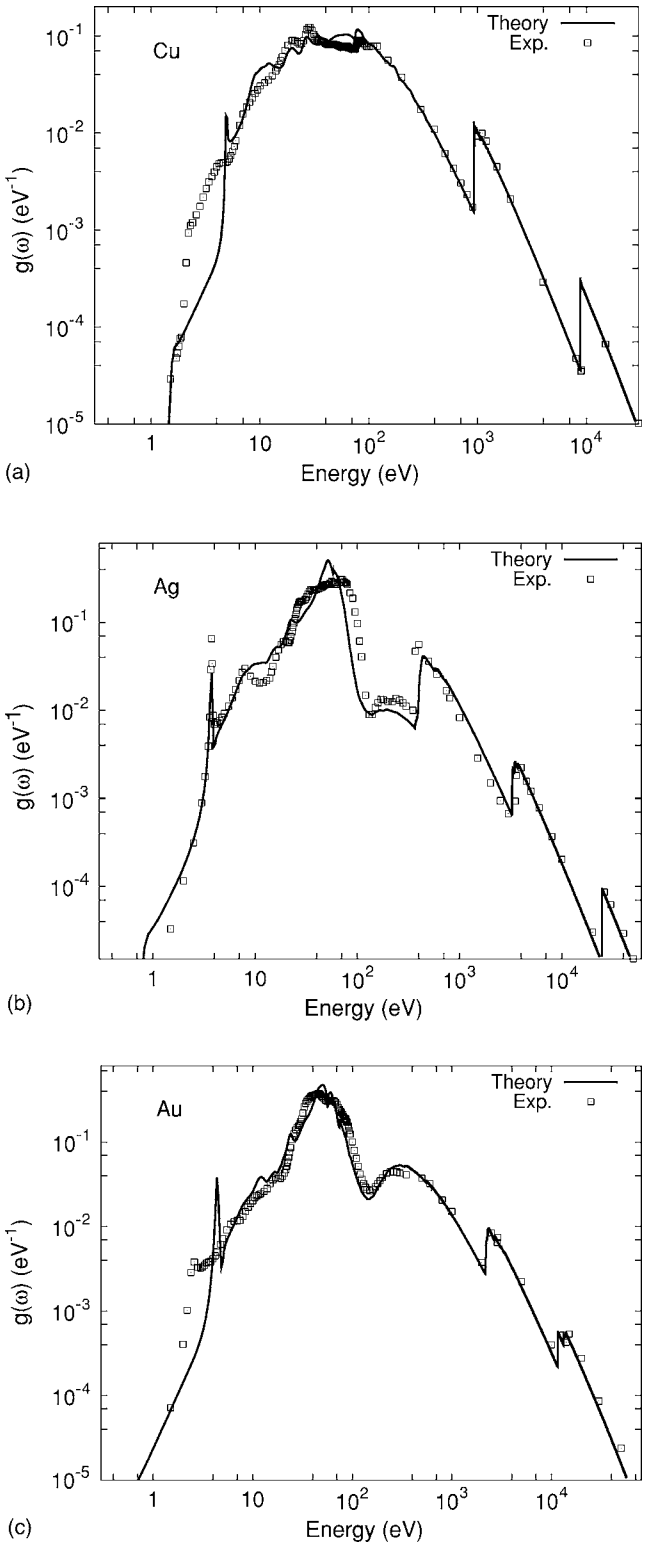

FIG. 2. Optical oscillator strengths for Cu (upper), Ag (middle), and Au (lower) as calculated in this work (solid) using the FEFF8OP code and compared to experiment (Refs. 23 and 24) (points).

tionality constant can be determined experimentally to give a semiempirical "rule of thumb" $I \approx 10Z$ (eV). In the high Z regime the agreement between theory and experiment appears to be only semiquantitative, but it should be mentioned that the ratio of I to Z is not in fact constant, but rather varies from ~9 to 11, and has been measured to be as low as 8.32 for lanthanum.[28] Furthermore, only the logarithm of I is needed for the determination of physical quantities, and typical errors in $\ln I$ from the values in Table I are only a few %. For example, for a typical case of 100 keV electrons in gold, the error in stopping powers calculated using experimental versus theoretical values of I is only around 2%. Furthermore, this error decreases as the incoming electron energy increases. On the other hand, at the lowest energy (e.g., ~10 keV for Au) where the Bethe formula (and the usefulness of $\ln I$ for calculating the CSP) is applicable, the difference between experimental and theoretical CSPs is still only around 6%. The method of calculating the CSP below the energy range where the Bethe formula is applicable and without directly using $\ln I$, is described in Sec. V.

TABLE I. Mean excitation energies I for several elements as calculated in this work, and for comparison, results calculated from experimental (Refs. 24 and 26) optical constants, and recommended (ICRU) values (Ref. 27).

Element	I theory (eV)	I expt. (eV)	ICRU (eV)
Aluminum	165	167 (Ref. 26), 162 (Ref. 24)	166
Silicon	174	173 (Ref. 26)	173
Copper	312	319 (Ref. 24)	322
Silver	420	382 (Ref. 24)	470
Gold	662	752 (Ref. 24)	790

In the IMFP calculations presented here, we consider two different extensions to finite q, as described below. Since our calculations show that both lead to similar results for the IMFP, we only present calculations of the CSP with one of these extensions. However, all our calculations use the same full-spectrum calculations of $\epsilon(\omega)$. For our IMFP calculations, we have used the many-pole representation of the dielectric function of Ref. 16, i.e., we approximate our calculated ELF $-\mathrm{Im}[\epsilon^{-1}(\omega)]$ as a sum of many (typically of order 100) discrete poles. This "many-pole" model, denoted by $\epsilon_N^{-1}(\omega)$, has the standard analytic form for dielectric response,

$$\epsilon_N^{-1}(\omega) = 1 + \sum_{j=1}^{N} g_j \frac{\omega_j^2}{\omega^2 - \omega_j^2 + i\omega\delta}, \tag{9}$$

where $\omega\delta$ is a small damping term, comparable to the pole separations. Figure 3 compares the IMFP for Cu as calculated using both our many-pole model and a single plasmon-pole model.[29] This single-pole model is essentially an Einstein model for the response in which excitations (for a given momentum transfer q) occur at the plasmon excitation energy ω_q. Thus the single-pole model is a special case of the many-pole model in which all but one of the weights g_j appearing in Eq. (9) are set to zero. In our many-pole representation, the parameters ω_j are taken to be evenly spaced along the energy-loss axis, and the weights g_j are fixed by matching our calculation of $\mathrm{Im}[\epsilon^{-1}(\omega)]$ according to the formula

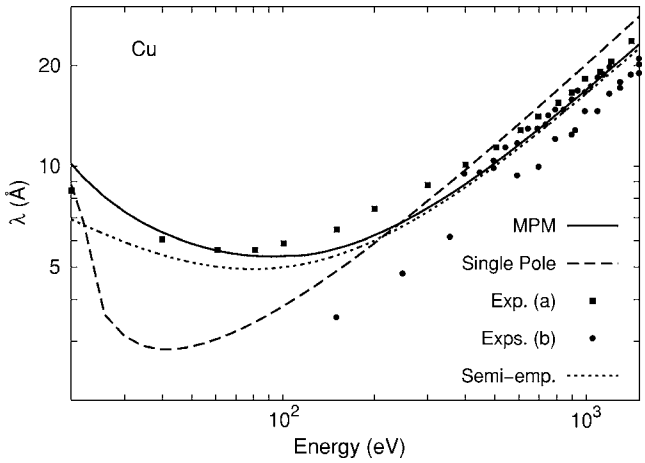

FIG. 3. The inelastic mean-free paths for copper calculated using the same *ab initio* dielectric function as the basis of two different theoretical models: the many-pole self-energy (MPM) model of Eq. (18) and the single-pole self-energy model (described in the text). These theoretical results are compared to: Expt. (a) Ref. 34 (squares); Expts. (b) (circles, the references for Expts. (b) are given in Ref. 5); and a semiempirical curve which is described in Ref. 5.

$$g_j = -\frac{2}{\pi}\frac{1}{\omega_j^2}\int_{\Delta_j} d\omega\omega\ \mathrm{Im}[\epsilon^{-1}(\omega)], \tag{10}$$

where the integration region Δ_j is from $(\omega_j+\omega_{j-1})/2$ to $(\omega_j+\omega_{j+1})/2$ and the similarity with Eq. (7) is apparent. Finally, the extension to finite q is obtained by shifting the pole locations via the substitution[29]

$$\omega_j^2 \to \omega_j^2 + \frac{v_F^2 q^2}{3} + \frac{q^4}{4}, \tag{11}$$

where v_F is the Fermi velocity as calculated at the mean interstitial electron density from the FEFF8 code. Further details of our approach, though not essential to our discussion here, are given in Refs. 16, 22, and 30. The above substitution is sufficient to induce the so-called "Bethe ridge" for large momentum transfer where the ELF is peaked about the point $\omega=q^2/2$. In other words, our model for large q satisfies the approximate relation

$$-\mathrm{Im}[\epsilon^{-1}(q,\omega)] \approx \pi\Omega_p^2\delta(\omega^2-Q^2), \tag{12}$$

where $Q\equiv q^2/2$. Consequently the above extension can be regarded as an interpolation formula between small and large Q.

For CSP calculations, our aim here is to replace experimental optical data (which is used as input in the ODM of Ref. 4) with theoretical optical data from our *ab initio* calculation of $\epsilon(\omega)$, i.e., with an *ab initio* data model (ADM). Thus for consistency we follow the formulation of Ref. 4 as closely as possible in comparisons with their CSP results. In particular we have also implemented their delta-oscillator [19,31] extension to finite q for our CSP calculations. For nonrelativistic probe electrons the delta-oscillator model extends $\epsilon(\omega)$ to finite q according to the relation

$$-\mathrm{Im}[\epsilon^{-1}(q,\omega)] = \pi\Omega_p^2\frac{Z(Q)}{Z}\delta(\omega^2-Q^2) - \mathrm{Im}[\epsilon^{-1}(\omega)]\theta(\omega-Q), \tag{13}$$

where $Z(Q)$ is the number of electrons that contribute to the zero momentum-transfer sum rule with upper energy limit Q,

$$Z(Q) = -\frac{2Z}{\pi\Omega_p^2}\int_0^Q d\omega\omega\ \mathrm{Im}[\epsilon^{-1}(\omega)]. \tag{14}$$

Because $Z(Q)$ approaches Z for large q, we see that the extension to finite q in Eq. (13) gives the Bethe ridge in much the same way as that of Eq. (12).

Although the finite-q extension algorithms in this paper differ somewhat, we do not expect our nonrelativistic results to depend substantially on the details. The reason is that both algorithms reduce to the correct long-wavelength limit for low q, and both give the correct Bethe ridge dispersion for high q. This expectation is supported by the IMFP results in Sec. IV. Moreover our results for the q dependence are roughly consistent with the explicit real-space calculations of $-\mathrm{Im}[\epsilon^{-1}(q,\omega)]$ at finite q of Soininen *et al.*[32]

III. ELECTRON SELF-ENERGY

Inelastic losses in the propagation of a fast charged particle can be expressed in terms of one-particle *self-energy* $\Sigma(E)$. This complex-valued quantity is a dynamically screened exchange-correlation contribution to the quasiparticle energy-momentum relation

$$E = \frac{p^2}{2} + \Sigma(E,p), \tag{15}$$

where p is the quasiparticle momentum. Our approach for calculating $\Sigma(E)$, which refers to the self-energy $\Sigma(E,p)$ on the energy shell where $E=E(p)$, is based on the "*GW*" approximation of Hedin,[33] together with our many-pole representation of the dielectric function, as summarized above.[16] In the *GW* method the vertex corrections to the electron self-energy are neglected, yielding an expression for $\Sigma(E)$ in terms of the electron propagator G and the screened Coulomb potential acting on an electron W, i.e.,

$$\Sigma(\mathbf{x},\mathbf{x}';E) = i\int\frac{d\omega}{2\pi}e^{-i\omega\eta}G(\mathbf{x},\mathbf{x}';E-\omega)W(\mathbf{x},\mathbf{x}';\omega), \tag{16}$$

where η is a positive infinitesimal and the $(\mathbf{x},\mathbf{x}')$ are spatial indices. Within the RSGF approach, the propagator G is calculated using a multiple-scattering expansion $G=G_0+G_0tG_0+\cdots$.[17] However, for simplicity in this work, we neglect the multiple-scattering terms (which would give rise to fluctuations in the self-energy) and simply use the free propagator G_0 for a homogeneous electron gas at the mean interstitial density. Then the screened Coulomb interaction for a spatially homogeneous system can be obtained from the Fourier transform $W(\mathbf{q},\omega)=\mathcal{F}[W(\mathbf{x}-\mathbf{x}',t)]$ and can be expressed in terms of the Coulomb potential $V_q=4\pi/q^2$ and the dielectric function $\epsilon(\mathbf{q},\omega)$ as

$$W(\mathbf{q},\omega) = \epsilon^{-1}(\mathbf{q},\omega)V_q. \tag{17}$$

The calculations of $\Sigma(E)$ are then carried out using the many-pole representation of Eqs. (9) and (11). With this homogeneous model, our calculated $\Sigma(E)$ is then the average self-energy in the system. Further details are given in Ref. 30.

IV. INELASTIC MEAN-FREE PATH

We first calculate Eq. (1) for the IMFP in terms of the excited state self-energy $\Sigma(E)$ of the fast electron.

$$\lambda(E) = \sqrt{\frac{E}{2}}\frac{1}{|\mathrm{Im}\,\Sigma(E)|}. \tag{18}$$

Eq. (18) for the IMFP is consistent with the decay of a single electron wave function whose time dependence is given by $e^{-iE(p)t}$.[36] Eq. (18) is also equivalent to Eq. (1) because the self-energy is proportional to the forward scattering amplitude, i.e.,

$$\mathrm{Im}\,\Sigma(\mathbf{p}) = -2\pi n_a\,\mathrm{Im}\,f(\mathbf{p},\mathbf{p}). \tag{19}$$

The equivalence of Eq. (1) and Eq. (18) then follows from the optical theorem. It should be noted, however, that our calculations of the IMFP in terms of the self-energy via Eq. (18) do not include relativistic effects, whereas Eq. (1) is fully relativistic.

The explicit dependence of the self-energy on the dielectric function in Eq. (17), the many-pole model of Eqs. (9) and (11), and the full-spectrum FEFF8OP code are all that are needed to carry out *ab initio* calculations of IMFPs according to Eq. (18). Our many-pole model IMFP calculations (labeled MPM) are shown for several materials in Figs. 3 and 4, together with best fits[5] to currently available data. The fit lines in Figs. 3 and 4 are based on multiple data sets which were taken up to 3000 eV and are expected to accurately describe the IMFP as low as 50 eV. Figure 4 also shows a calculation (labeled "ADM") which uses our *ab initio* $\epsilon(\omega)$ as input data to the semiempirical optical-data model of Ref. 4. Note that the MPM and ADM results are in good agreement with each other, which verifies that the different extensions to finite q discussed in Sec. II do not lead to substantially different results. Both theoretical models are plotted here over the expected range of validity of the fit line, but can be extended with our codes to energies up to ~100 keV. Although the agreement with experiment is reasonable, our calculations tend to underestimate the experimental IMFP somewhat for high Z materials.

V. STOPPING POWER

As noted in the Introduction the CSP is the net reaction force $S(E)=-dE/dx$ due to electronic collisions at a given energy E that slows a fast probe electron. Over the range of energies from about 10 eV up to about 10 MeV, the CSP is the main contribution to the total stopping power. Above this energy the total stopping power may be dominated by bremsstrahlung.[27] The CSP is calculated in this work using Eq. (2), where the DCS is related to our *ab initio* ELF, using

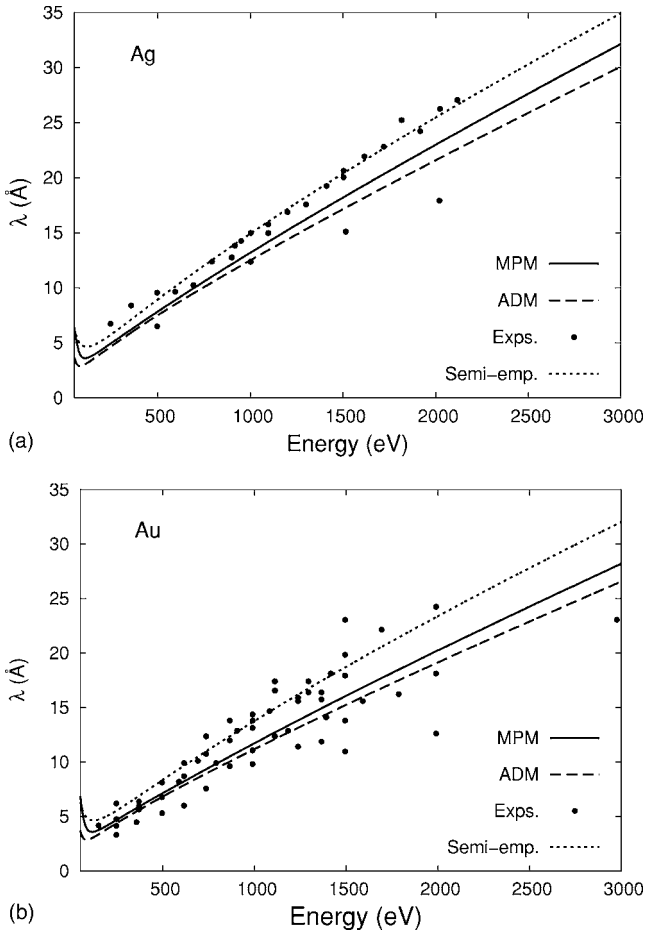

FIG. 4. The inelastic mean-free paths for Ag (upper) and Au (lower) calculated using the same *ab initio* dielectric function as the basis for two different theoretical models: the many-pole self-energy (MPM) model of Eq. (18), and the *ab initio* data model (ADM) described in the Introduction. The theoretical results are compared to a semiempirical curve (Ref. 5) and to multiple experimental data sets. The references for the Expts. are given in Ref. 5. The theoretical models are plotted over the expected range of validity of the semiempirical curve.

the formulation of Ref. 4. This model is thought to be applicable with confidence for energies above ~100 eV, and appears to be applicable as low as ~10 eV. However, it is not obvious why a model based on the first Born approximation should be valid at such low energies. Furthermore, in the Born approximation the CSP is proportional to the square of the incoming particle charge and thus nonlinear corrections such as the Barkas effect[15] are not included in this model. In the relativistic limit Eq. (2) reduces to the well-known Bethe formula[1–3,37] for the stopping power

$$S(E) = \frac{\pi}{2}\frac{\Omega_p^2}{v^2}\left[\ln\left(\frac{E^2}{I^2}\frac{\gamma+1}{2}\right) + F(\gamma) - \delta_F(\gamma)\right], \tag{20}$$

where $\gamma=(1-v^2/c^2)^{-1/2}$ is the relativistic dilation factor, and $F(\gamma)$ is given by

$$F(\gamma) = \left[\frac{1}{\gamma^2} - \frac{2\gamma-1}{\gamma^2}\ln 2 + \frac{1}{8}\left(\frac{\gamma-1}{\gamma}\right)^2\right]. \tag{21}$$

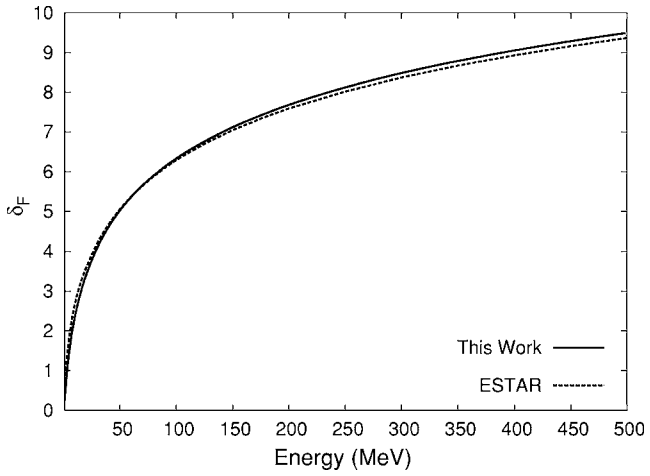

FIG. 5. Fano's density effect correction to the stopping power from Eq. (20) as calculated in this work (solid), and compared to semiempirical values (Ref. 38) for copper (dashes).

Also appearing in Eq. (20) are the "mean excitation energy" I defined in Sec. II, and Fano's density correction[3] δ_F. The density correction δ_F is due solely to transverse interactions, and can be neglected for nonrelativistic particles. A detailed description of how δ_F can be calculated as a functional of the ELF, is given in Ref. 4. Figure 5 shows the density correction $\delta_F(E)$ for copper as calculated using our *ab initio* dielectric function, and for comparison, the semiempirical values used by ESTAR.[38] ESTAR is an on-line implementation of Eq. (20) which takes semiempirical values of I as input. The mean excitation energy and the density correction have, heretofore, been difficult to calculate from first principles, as they require accurate values of the OOS over a very large energy spectrum. However, our full-spectrum approach clearly gives reasonable agreement with experiment.

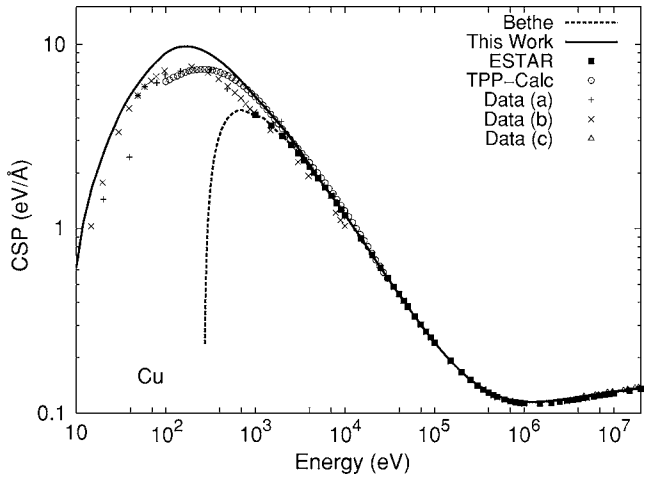

FIG. 6. Collision stopping power for Cu as calculated using the *ab initio* dielectric function of this work (solid) in the ADM (see text). Also shown are semiempirical values of the CSP from ESTAR (Ref. 38) (solid squares), and semiempirical CSP values (labeled TPP-calc) based on the Penn model (Ref. 35) (circles), and CSP values from experimental data: (+), (Ref. 39) (×), (Ref. 40) and (triangles) (Ref. 41). The Bethe formula of Eq. (20) is shown as a dashed line.

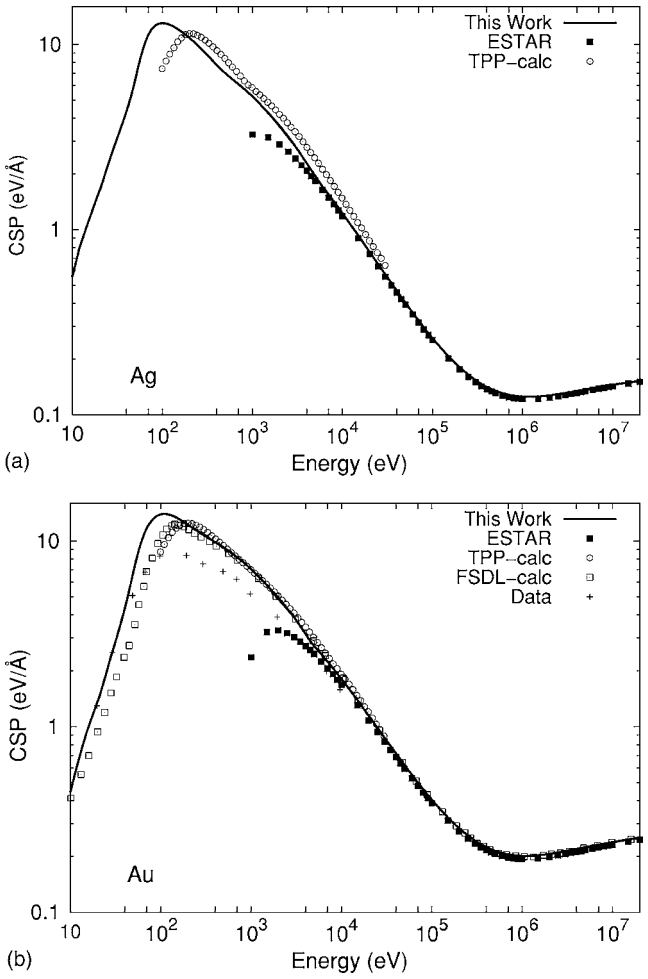

FIG. 7. The collision-stopping powers for Ag (upper) and Au (lower), with labels as in Fig. 6. Also shown for Au are the semiempirical CSP values as calculated in Ref. 4 (labeled FSDL-calc), and CSP values from experiment (Ref. 39).

For relativistic probe electrons, the excellent agreement of the Bethe formula in Eq. (20) for the CSP is well known, so we have included data from ESTAR in lieu of experiment where necessary. The difference between Eq. (20) and Eq. (2) only appears in the nonrelativistic regime, and can be seen in Fig. 6, where Eq. (20) begins to fail around 5000 eV. In order to calculate CSPs that are in good agreement with experiment for both nonrelativistic and relativistic probe electrons we apply Eq. (2) with the more general form of $d\sigma/d\omega$ given in Ref. 4, but using our calculated dielectric function as input are in good agreement with the ESTAR results. Figure 6 shows our results for the calculated CSP for high energy electrons for Cu. Similarly Fig. 7 shows results for Ag and Au. Clearly these results are in good agreement with the ESTAR results. However, for energies lower than about 1 keV, the CSP calculations of this work show significantly better agreement with data than those obtained with the Bethe formula.

Empirically the CSP falls off approximately as a power law of the energy over a few decades beyond the peak loss,

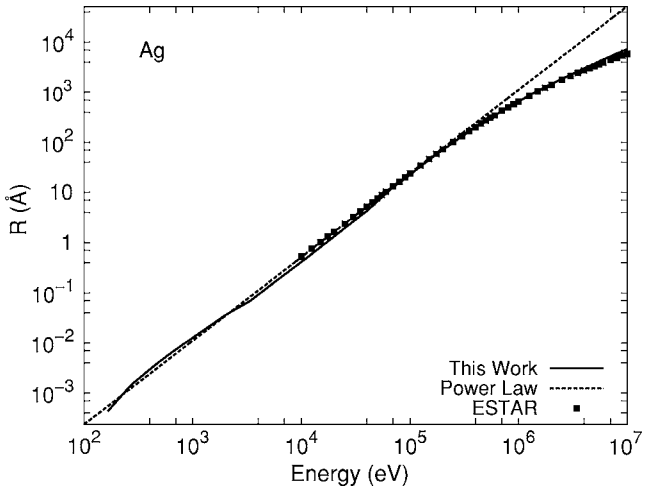

FIG. 8. The CSDA range $R(E)$ as given by Eq. (3) for electrons in silver as calculated in this work (solid), and compared to ESTAR (squares), and to a pure power-law $R(E)=0.271E^{5/3}$ (dashes) with E in Hartrees.

but before the transverse effects take over. Because of this, the range $R(E)$ can also be approximated as a power law. However, our calculations show that there are deviations from a pure power-law dependence, as shown in Fig. 8 for silver, and compared with our full calculation and ESTAR.

VI. CONCLUSIONS

We have presented a general real-space Green's function approach for *ab initio* calculations of inelastic losses and stopping powers in condensed matter. Unlike most current approaches, our method is based on first-principles calculations of dielectric response, and does not rely on empirical optical data. We also find that accurate calculations of inelastic losses of probe electrons depend primarily on the quality of the calculated $q=0$ dielectric function, and not on the details of the extension to finite q. Using our *ab initio* dielectric function, we also calculate the mean excitation energy and stopping powers for relativistic electrons, obtaining results in good agreement with experimental data. Furthermore, using the *ab initio* ADM we can extend the stopping power calculation down to energies of ~10 eV, i.e., much lower than the Bethe formula, while still maintaining reasonable agreement with experiment. Our approach for calculating inelastic losses of probe electrons can be easily extended to probe positrons. In conclusion, we believe our approach has the potential to complement or provide an alternative to semiempirical approaches for calculations of IMFPs and stopping powers of electrons in condensed matter.

ACKNOWLEDGMENTS

We wish to thank G. Bertsch, H. Bichsel, J. M. Fernández-Varea, C. Powell, P. Rez, and E. Stern for comments and suggestions. This work is supported in part by the DOE Grant No. DE-FG03-97ER45623 (JJR) NIH NCRR BTP Grant No. RR-01209 (JJK), and NIST Grant No. 70 NAMB 2H003 (APS) and was facilitated by the DOE Computational Materials Science Network.

[1] H. A. Bethe, Ann. Phys. **5**, 325 (1930) (this paper is reviewed in Ref. 37).
[2] E. Fermi, Phys. Rev. **57**, 485 (1940).
[3] U. Fano, Annu. Rev. Nucl. Sci. **13**, 1 (1963).
[4] J. M. Fernández-Varea, F. Salvat, M. Dingfelder, and D. Liljequist, Nucl. Instrum. Methods Phys. Res. B **229**, 187 (2005).
[5] C. J. Powell and A. Jablonski, J. Phys. Chem. Ref. Data **28**, 19 (1999).
[6] H. Bichsel, in *Atomic, Molecular, and Optical Physics Handbook*, edited by G. W. F. Drake (AIP Press, Woodbury, N.Y., 1996).
[7] I. Campillo, J. M. Pitarke, A. Rubio, E. Zarate, and P. M. Echenique, Phys. Rev. Lett. **83**, 2230 (1999).
[8] J. A. Soininen, J. J. Rehr, and E. L. Shirley, J. Phys.: Condens. Matter **15**, 2573 (2003).
[9] D. R. Penn, Phys. Rev. B **35**, 482 (1987).
[10] R. M. Sternheimer, S. M. Seltzer, and M. J. Berger, Phys. Rev. B **26**, 6067 (1982).
[11] R. M. Sternheimer, S. M. Seltzer, and M. J. Berger, Phys. Rev. B **27**, 6971 (1983).
[12] I. Abril, R. Garcia-Molina, C. D. Denton, F. J. Pérez-Pérez, and N. R. Arista, Phys. Rev. A **58**, 357 (1998).
[13] S. Heredia-Avalos, R. Garcia-Molina, J. M. Fernández-Varea, and I. Abril, Phys. Rev. A **72**, 052902 (2005).
[14] C. C. Montanari and J. E. Miraglia, Phys. Rev. A **73**, 024901 (2006).
[15] P. Sigmund and A. Schinner, Nucl. Instrum. Methods Phys. Res. B **212**, 110 (2003).
[16] J. J. Rehr, J. J. Kas, M. P. Prange, F. D. Vila, A. L. Ankudinov, L. W. Campbell, and A. P. Sorini, cond-mat/0601241 (unpublished).
[17] A. L. Ankudinov, B. Ravel, J. J. Rehr, and S. D. Conradson, Phys. Rev. B **58**, 7565 (1998).
[18] M. Prange, G. Rivas, J. Rehr, and A. Ankudinov (unpublished).
[19] D. Liljequist, J. Phys. D **16**, 1567 (1983).
[20] J. C. Ashley, J. J. Cowan, R. H. Ritchie, V. E. Anderson, and J. Hoelzl, Thin Solid Films **60**, 361 (1979).
[21] J. C. Ashley, J. Electron Spectrosc. Relat. Phenom. **46**, 199 (1988).
[22] M. Prange, G. Rivas, and J. J. Rehr, *Table of Optical Constants for Mg, Al, Cu, Ag, Au, Bi and C.* (World Wide Web, http://leonardo.phys.washington.edu/feff/opcons/, 2005).
[23] H. J. Hagemann, W. Gudat, and C. Kunz, J. Opt. Soc. Am. **65**, 7421 (1975).
[24] H. J. Hagemann, W. Gudat, and C. Kunz, *Optical Constants from the Far Infrared to the X-ray Region: Mg, Al, Cu, Ag, Au, Bi, C and* Al_2O_3*, DESY SR-7417* (Desy, Hamburg, West Germany, 1974).
[25] A. P. Sorini, J. Kas, J. J. Rehr, and M. P. Prange, *Tables of mean free paths and stopping powers* (World Wide Web, http://leonardo.phys.washington.edu/feff/loss/, 2005).

[26] C. Tschalar and H. Bichsel, Phys. Rev. **175**, 476 (1968).
[27] *ICRU Report* 37, *Stopping Powers and Ranges for Protons and Alpha Particles* (International Commission of Radiation Units and Measurements, 1984).
[28] H. Bichsel, Phys. Rev. A **46**, 5761 (1992).
[29] B. Lundqvist, Phys. Kondens. Mater. **6**, 193 (1967).
[30] J. Kas, A. Sorini, M. Prange, and J. Rehr (unpublished).
[31] F. Salvat, J. M. Fernández-Varea, and J. Sempau, *PENELOPE - A Code System for Monte Carlo Simulation of Electron and Photon Transport* (OECD/Nuclear Energy Agency, Issy-les-Moulineaux, France, http://www.nea.fr, 2003).
[32] J. A. Soininen, A. L. Ankudinov, and J. J. Rehr, Phys. Rev. B **72**, 045136 (2005).
[33] L. Hedin and S. Lundqvist, Solid State Phys. **23**, 1 (1969).
[34] W. S. M. Werner, Surf. Interface Anal. **31**, 141 (2001).
[35] S. Tanuma, C. J. Powell, and D. R. Penn, Surf. Interface Anal. **37**, 978 (2005).
[36] J. J. Quinn, Phys. Rev. **126**, 1453 (1962).
[37] M. Inokuti, Rev. Mod. Phys. **43**, 297 (1971).
[38] M. J. Berger, J. S. Coursey, M. A. Zucker, and J. Chang, *ESTAR, PSTAR, and ASTAR: Computer Programs for Calculating Stopping-Power and Range Tables for Electrons, Protons, and Helium Ions (version 1.2.3)* (National Institute of Standards and Technology, Gaithersburg, MD., http://physics.nist.gov/Star, 2005).
[39] S. Luo, X. Zhang, and D. C. Joy, Radiat. Eff. Defects Solids **117**, 235 (1991).
[40] P. Hovington, D. C. Joy, R. Gauvin, and N. Evans, Scanning Microsc. **10**, 653 (1996).
[41] M. S. Macpherson, Ph.D. thesis, Carleton University, NRC Report PIRS-0626 (1998).